



HAL
open science

Variations of petrophysical properties and spectral induced polarization in response to drainage and imbibition: a study on a correlated random tube network

Alexis Maineult, Damien Jougnot, André Revil

► **To cite this version:**

Alexis Maineult, Damien Jougnot, André Revil. Variations of petrophysical properties and spectral induced polarization in response to drainage and imbibition: a study on a correlated random tube network. *Geophysical Journal International*, 2018, 212 (2), pp.1398-1411. 10.1093/gji/ggx474. hal-02324290v2

HAL Id: hal-02324290

<https://hal.science/hal-02324290v2>

Submitted on 21 Oct 2019

HAL is a multi-disciplinary open access archive for the deposit and dissemination of scientific research documents, whether they are published or not. The documents may come from teaching and research institutions in France or abroad, or from public or private research centers.

L'archive ouverte pluridisciplinaire **HAL**, est destinée au dépôt et à la diffusion de documents scientifiques de niveau recherche, publiés ou non, émanant des établissements d'enseignement et de recherche français ou étrangers, des laboratoires publics ou privés.

Variations of petrophysical properties and spectral induced polarization in response to drainage and imbibition: a study on a correlated random tube network

Alexis Mainault,¹ Damien Jougnot¹ and André Revil^{2,3}

¹*Sorbonne Universités, UPMC Univ Paris 06, CNRS, EPHE, UMR 7619 Metis, 4 place Jussieu, 75005 Paris, France. E-mail: alexis.mainault@upmc.fr*

²*Univ. Grenoble Alpes, CNRS, IRD, IFSTTAR, ISTerre, 38000 Grenoble, France*

³*Univ. Savoie Mont Blanc, ISTerre, 73000 Chambéry, France*

Accepted 2017 October 31. Received 2017 October 30; in original form 2017 April 21

SUMMARY

We implement a procedure to simulate the drainage and imbibition in random, 2-D, square networks. We compute the resistivity index, the relative permeability and the characteristic lengths of a correlated network at various saturation states, under the assumption that the surface conductivity can be neglected. These parameters exhibit a hysteretic behaviour. Then, we calculate the spectral induced polarization (SIP) response of the medium, under the assumption that the electrical impedance of each tube follows a local Warburg conductivity model, with identical DC conductivity and chargeability for all the tubes. We evidence that the shape of the SIP spectra depends on the saturation state. The analysis of the evolution of the macroscopic Cole–Cole parameters of the spectra in function of the saturation also behaves hysteretically, except for the Cole–Cole exponent. We also observe a power-law relationship between the macroscopic DC conductivity and time constant and the relative permeability. We also show that the frequency peak of the phase spectra is directly related to the characteristic length and to the relative permeability, underlining the potential interest of SIP measurements for the estimation of the permeability of unsaturated media.

Key words: Electrical properties; Permeability and porosity; Hydrogeophysics; Numerical modelling.

1 INTRODUCTION

Geophysical methods are now commonly used to characterize the hydrological state of the subsurface, for instance to localize aquifers (e.g. Vereecken *et al.* 2006; Hubbard & Linde 2011; Binley *et al.* 2015) and to determine their hydraulic conductivity and storage coefficient distributions (e.g. Soueid Ahmed *et al.* 2016a,b). Electrical resistivity tomography provides some information regarding the architecture of the subsurface (e.g. Binley & Kemna 2005; Johnson *et al.* 2010) and this method is sensitive to the water content, temperature, salinity and cation exchange capacity (Shainberg *et al.* 1980; Sen *et al.* 1981). To date, one remaining challenge for field hydrogeophysicists is to be able to estimate, in a reliable way, the saturation state of the medium and its permeability at partial saturation, which are parameters of importance for the characterization of the vadose zone (Doussan & Ruy 2009).

In the past decade, the induced polarization (IP) method has shown its potential to estimate the permeability in saturated conditions (Slater & Lesmes 2002; Tong *et al.* 2004; Binley *et al.* 2005; Hördt *et al.* 2007; Weller *et al.* 2010; Attwa & Günther 2013; Slater *et al.* 2014; Revil *et al.* 2015). Laboratory studies have also evidenced that some characteristics of the IP response are di-

rectly modified when the saturation is changed (e.g. Titov *et al.* 2004; Cosenza *et al.* 2007; Jougnot *et al.* 2010; Breede *et al.* 2011; Schmutz *et al.* 2012).

The spectral induced polarization (SIP) method consists in injecting a sinusoidal electrical current $I = I_0 \sin(\omega t)$ (ω is the pulsation frequency and t the time) in the medium with two injection electrodes, and simultaneously measuring the resulting electrical potential ΔV between two measurement electrodes. The complex conductivity spectrum is obtained by repeating the measurement for different frequencies and is given by

$$\sigma^*(\omega) = \frac{1}{G} \frac{I^*(\omega)}{\Delta V^*(\omega)} = \frac{1}{G} \frac{|I^*(\omega)|}{|\Delta V^*(\omega)|} e^{-i\varphi(\omega)} = \sigma(\omega) e^{-i\varphi(\omega)} \quad (1)$$

where the superscript * denotes a complex quantity. Here σ^* stands for complex conductivity, σ for the conductivity amplitude, φ for the phase, G for the geometrical factor determined from the electrode locations and the boundary conditions and i for the pure imaginary number. The method of random tube networks has long been applied to study the permeability and the formation factor (e.g. Kirkpatrick 1973; Koplik 1981; David *et al.* 1990; David 1993; Bernabé 1995). Recently, Mainault *et al.* (2017) used the method to study the up-scaling of the SIP response, from pore scale to sample scale and

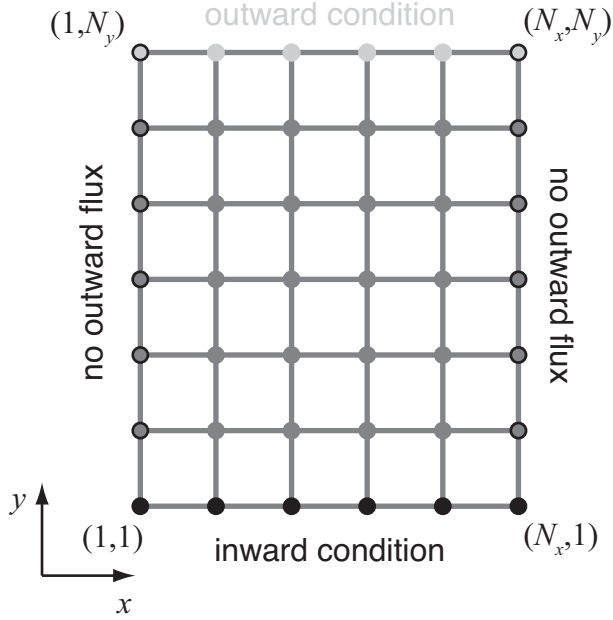


Figure 1. Scheme of a 2-D square tube network for the computation of the macroscopic complex conductivity (CC), apparent formation factor (AFF) and apparent hydraulic permeability (AHP). There are no outflowing fluxes on the lateral faces (nodes $x = 1$ and $x = N_x$). The inward condition (nodes $y = 1$) is a potential equal to $V_0 e^{i\omega t}$ for CC, and 1 for AFF and AHP. The outward condition (nodes $y = N_y$) is a potential equal to 0 in the three cases.

to analyse the relationship between the pore size distribution and the dispersion shown by the complex conductivity spectra. Briefly, a sinusoidal current is applied between the two end-faces of a 2-D square network (Fig. 1), made of a set of connected capillaries with identical length but different radius (Figs 2a and b). The conservation law for the complex electrical current (Kirchhoff 1845) can be written at each node. Knowing the complex impedance of each tube, this produces a linear system whose resolution gives the complex electrical potential at each node. From the electrical potential and the tube impedances, the macroscopic current entering in or exiting from the system (note that they are equal) can be deduced. The complex conductivity is then computed using

eq. (1) (G is equal to 1 in this case). To summarize, this methodology allows the macroscopic impedance of a set of local impedances to be calculated (Fig. 2c). In this paper, we apply the same methodology to study the effect of a desaturation process (i.e. drainage) and then a resaturation process (i.e. imbibition) on the macroscopic SIP response of the network.

2 METHOD

We consider the 100×100 (i.e. 19 800 tubes) network of Fig. 2(a), for which the logarithm of the pore radius distribution r is normally distributed, with a mean radius of $10 \mu\text{m}$ and a standard deviation of 0.4942. All tubes have the same length l . The medium is correlated, with a Hurst exponent (related to the fractal dimension of the medium, e.g. Turcotte 1997) of 0.9, and an isotropic characteristic length scale of 1. It corresponds to the correlated medium used in Mainault *et al.* (2017, their fig. 5). In the present work, we consider the effect of partial saturation on the upscaled SIP response. By applying the Young–Laplace equation, it is possible to relate an equivalent radius r_{eq} (in m) that drains at a specific matric potential by (e.g. Jurin 1717)

$$h = \frac{2\gamma \cos \theta}{\rho_w g r_{\text{eq}}}, \quad (2)$$

where h is the matric potential (in m), γ is the surface tension of water (0.0727 N m^{-1} at 20°C), θ is the contact angle (often considered to be 0° , which yields $\cos \theta = 1$, see Bear 1972), ρ_w is the water density (in kg m^{-3}), and g is the gravitational acceleration (in m s^{-2}). This approach is traditionally used in soil science, when using simplified geometries to study the effect of water saturation upon effective properties: for hydrodynamic properties (e.g. Jury *et al.* 1991; Or & Tuller 1999; Guarracino 2007), hysteresis (e.g. Soldi *et al.* 2017), electrical conductivity (e.g. Niu *et al.* 2015) or self-potential (e.g. Packard 1953; Jougnot *et al.* 2012). However, given that the geometry of the porous medium is here known, we applied specific desaturation and resaturation processes that are described below and in Fig. 3. The hysteretic nature of the soil–water retention curve yields to different water content at a given matric potential during desaturation or resaturation of porous media (e.g. Mualem 1973). This hysteresis can be explained by different physical effects such as pore throats (‘ink-bottle’ effect), entrapped air, and possible

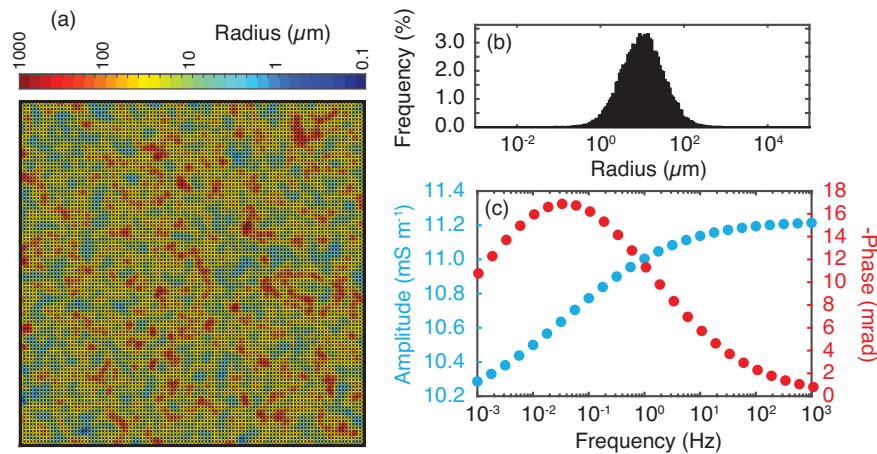


Figure 2. (a) 100×100 studied correlated network used in this study (the decimal logarithm of the radii is normally distributed, with a mean radius of $10 \mu\text{m}$ and a standard deviation of 0.4942, a Hurst exponent of 0.9, and a characteristic scale L_c of 1), (b) associated radius distribution, and (c) macroscopic complex conductivity response of the network (for a Warburg model with a DC conductivity of 10 mS m^{-1} , a chargeability of 0.1, and a diffusion coefficient of $10^{-11} \text{ m}^2 \text{ s}^{-1}$). See Mainault *et al.* (2017) for more details.

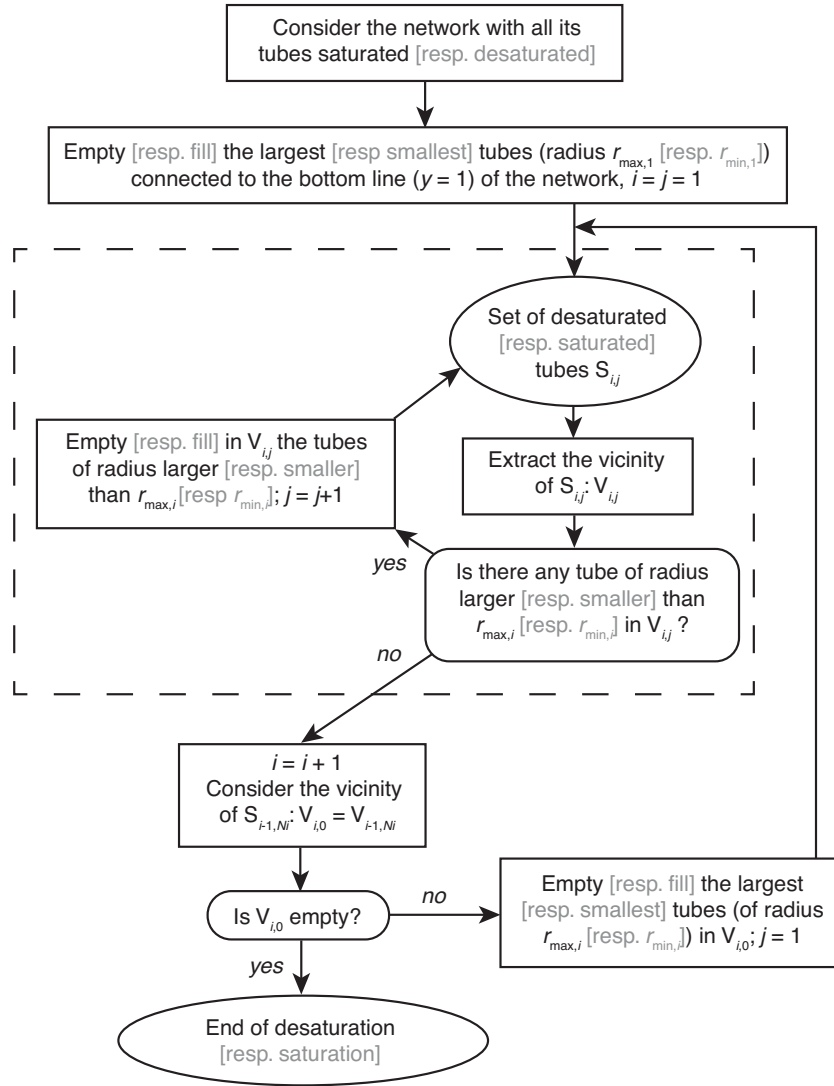


Figure 3. Diagram explaining the saturation and desaturation (grey words) of the network.

changes in the contact angle of advancing or receding meniscus (see Pham *et al.* 2005 for a review). In this study, we consider the so-called ‘ink-bottle’ effect: that is, parts of the network are not accessible to air or water entry due the pore size distribution as a result of eq. (2).

2.1 Desaturation of the tube network

Concerning drainage (desaturation), we consider the network initially fully saturated with water (Fig. 4a, saturation S_w of 100 per cent). We start the desaturation process from the bottom of the network (nodes $y = 1$, Fig. 1), by emptying the largest tubes (or the largest tube, if there is only one) connected to this face. We denote their radius $r_{\max,1}$, and the set of the so emptied tubes $S_{1,1}$ (step 0). We then consider the vicinity $V_{1,1}$ of $S_{1,1}$, that is, the set of tubes connected to $S_{1,1}$; we empty the tubes with a radius larger than or equal to $r_{\max,1}$ in $V_{1,1}$, to obtain $S_{1,2}$ (step 1). We continue the same process until the number of emptied tubes does not increase anymore. We note the set of emptied tubes after stabilization $S_{1,N1}$ (last step). To empty a tube, we just set its radius to 0, so the water

saturation associated to the radius $r_{\max,1}$ is simply computed at the end of the last step as:

$$S_w(r_{\max,1}) = \frac{\sum_{i=1}^{N_t} r_i^2}{\Sigma_0} \quad (3)$$

where Σ_0 is the sum of the squared radii for the complete network (i.e. at 100 per cent saturation), and N_t the total number of tubes. Afterwards, we consider the vicinity of $S_{1,N1}$, that is, $V_{1,N1} = V_{2,0}$. We empty in $V_{2,0}$ the largest tubes, whose diameter, denoted $r_{\max,2}$, is obviously smaller than $r_{\max,1}$. We repeat the procedure from step 1 to the last step to obtain $S_{2,N2}$. Finally, the entire process is repeated until the network is totally emptied.

Different desaturation states are shown in Fig. 4. The desaturated zone forms clusters, which can appear very suddenly, when zones with radii largest than $r_{\max,M}$ are connected to emptied tubes with radius equal to $r_{\max,M}$. This phenomenon is known as ‘Haines jumps’ (e.g. Haine 1930; DiCarlo *et al.* 2003; Haas & Revil 2009; Berg *et al.* 2013): when the air passes from a pore throat to a wider pores and displaces water, it generate a sudden drop in capillary pressure (see also Fig. 6, on which the drops are clearly visible).

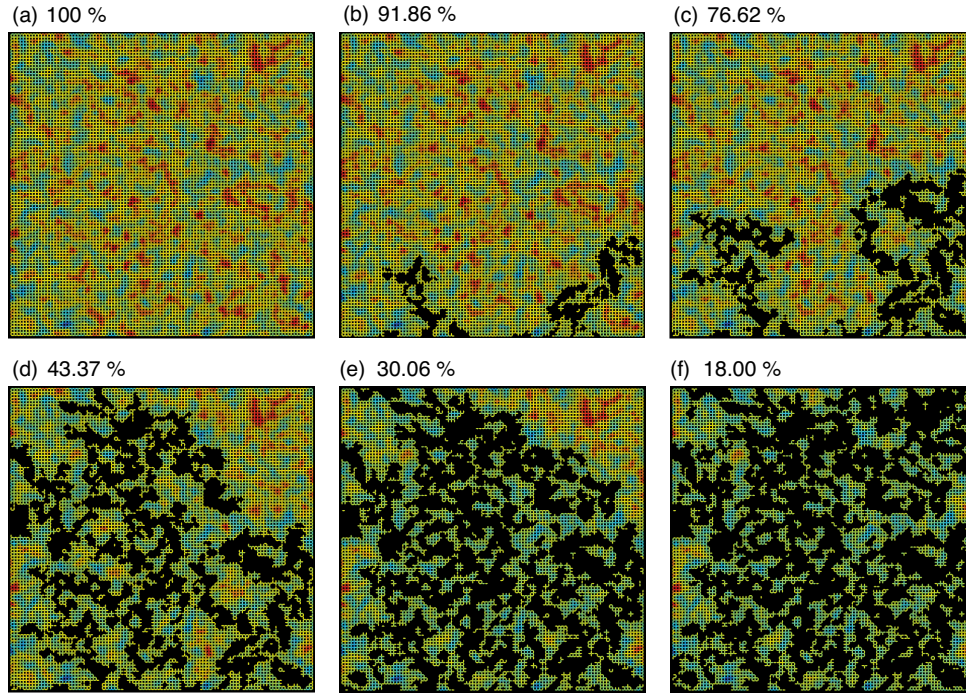


Figure 4. Example of saturation states during drainage. The largest radii are desaturated first (i.e. they are set to 0), starting from the bottom of the network (i.e. nodes $y = 1$, see Fig. 1). The colour scale is the same as in Fig. 2(a).

Also, there is a critical saturation for which two opposite end-faces are disconnected (i.e. there is no continuous path for the wetting phase between them)—in this case, 30.06 per cent in the transversal direction (between faces $x = 1$ and $x = 100$, see Fig. 1), and 18 per cent in the longitudinal direction (between faces $y = 1$ and $y = 100$). This difference is due to the fact that the desaturation process occurs along the longitudinal direction.

Finally, note that we continue the drainage process until $S_w = 0$, that is to say we do not consider water trapping in the tubes (their local saturation is 1 or 0), or in disconnected clusters of tubes. The desaturation process that we consider here is therefore similar to what we could obtain by putting the end-face $y = 1$ under vacuum.

2.2 Saturation of the tube network

For the imbibition (saturation), we start from a network with all its radii set to 0. Again, we start the saturation process from the bottom of the network (nodes $y = 1$, Fig. 1). We open the smallest tubes (or the smallest tube, if there is only one) connected to this face—we denote their radius $r_{\min,1}$, and the set of opened tubes is expressed as $S_{1,1}$ (step 0). Considering the vicinity $V_{1,1}$ of $S_{1,1}$, we open the tubes with a radius smaller or equal to $r_{\min,1}$ in $V_{1,1}$, to obtain $S_{1,2}$ (step 1). As for drainage, we continue the process until the set of opened tubes stabilizes (last step). The water saturation associated to $r_{\min,1}$ is also computed using eq. (3). Then, considering the vicinity $V_{2,0} = V_{1,N1}$, we opened in it the smallest tubes, of diameter $r_{\min,2}$ (which is larger than $r_{\min,1}$), and repeat the procedure from step 1 to the last step, and so on, until the network is totally opened and thus fully saturated. Note that we do not consider air trapping here: the saturation process is similar to what we could obtain by putting the end face $y = 1$ under high fluid pressure or by first saturating the medium with gas that is easy to dissolve in the water, as it is often done in soil physics. Examples of saturation states are shown in Fig. 5. Again, there is a critical saturation for which the

opposite end-faces connect: around 8.38 per cent in the longitudinal direction, and 13 per cent for the transversal direction.

2.3 Relative permeability, resistivity index and characteristic lengths

As pore network modelling is a well-known method (see for instance Kirkpatrick 1973; Koplik 1981; David *et al.* 1990; David 1993; Bernabé 1995), we just give in the appendix a summary of the approach. Using it, we compute: (i) the relative permeability k_r of the medium (the permeability at partial saturation being given by $k_r k$, with k the permeability at full saturation), (ii) the resistivity index RI , defined as the ratio of the electrical resistivity of the medium at partial saturation divided by the resistivity at full saturation (Archie 1942)—note that we have neglected the surface conductivity in computations, that is, only the conductivity of the fluid is taken into account, and (iii) The characteristic lengths Λ_h (hydraulic) and Λ_e (electrical) (in m; Johnson *et al.* 1986; Schwartz *et al.* 1989; Bernabé & Revil 1995), which can be seen as effective pore radii, and which are widely used parameters in petrophysics to link electrical conductivity and permeability (e.g. Schwartz *et al.* 1989; Bernabé & Revil 1995). In an electrical conductivity experiment, the length scale Λ_e denotes an effective pore radius weighted by the norm of the normalized electrical field in absence of surface conductivity (i.e. weighted by the local electrical field normalized by the applied electrical field in absence of surface conductivity, e.g. Avellaneda & Torquato 1991, and references therein).

2.4 Computation of the SIP spectra

To compute the SIP spectra of the networks at different saturation states, we used exactly the same approach as Mainault *et al.* (2017), and we modify the numerical scheme to account for tubes having radius equal to 0 (i.e. local impedance equal to 0). The local

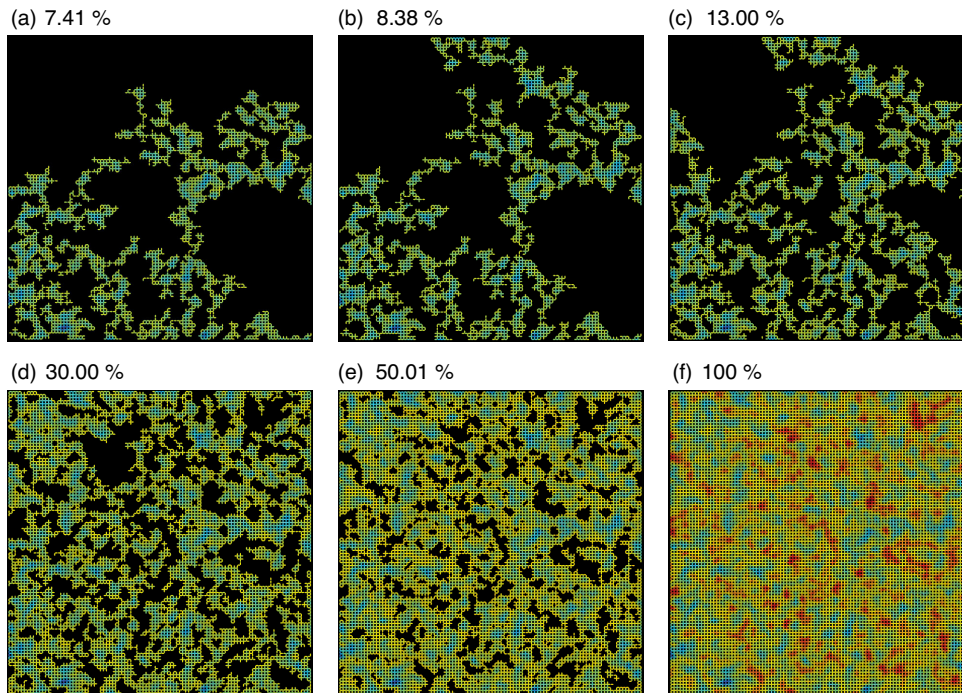


Figure 5. Example of saturation states during imbibition. The smallest radii are saturated first (i.e. all the radii where set to 0 at the initial state, and they are progressively set to their true value), starting from the bottom of the network (i.e. nodes $y = 1$, see Fig. 1). The colour scale is the same as in Fig. 2(a).

impedance of each tube of radius r non equal to 0 is given by a Warburg resistivity model written here in its complex conductivity form (Revil *et al.* 2014b; Niu & Revil 2016):

$$\sigma_l^* = \sigma_{0,l} \left(1 + \frac{m_l}{1 - m_l} \left(1 - \frac{1}{1 + (i\omega\tau_l)^{1/2}} \right) \right) \quad (4)$$

with

$$\tau_l = \frac{r^2}{2D_l}. \quad (5)$$

Note that this model is equivalent to a Warburg conductivity model using the relationship found in Tarasov & Titov (2013) between such functions. The rationale for a Warburg mode has been explored in details in Revil *et al.* (2014b) and Niu & Revil (2016) and will not be repeated here. The conductivity $\sigma_{0,l}$ denotes the DC conductivity (in S m^{-1}), m_l is the chargeability (dimensionless, comprised between 0 and 1), equal to $(\sigma_{\infty,l} - \sigma_{0,l})/\sigma_{\infty,l}$ where $\sigma_{\infty,l}$ is the limit of σ_l^* for infinite frequency, τ_l is the time constant (in s), and D_l is the diffusion coefficient of the counterions (Revil *et al.* 2012; Niu & Revil 2016). When a tube has a radius equal to 0 (desaturated state), we obtain $\sigma_l^* = 0$ by imposing $\sigma_{0,l} = 0$. As done by Maineult *et al.* (2017), we simplify the problem by imposing $\sigma_{0,l} = 0.01 \text{ S m}^{-1}$, $m_l = 0.1$ and $\log_{10}(D_l) = -11$ for all tubes with non-zero radius.

Once all the local impedances are attributed, we compute the complex conductivity spectra. Then we fit them with a macroscopic Pelton model in conductivity, which expresses the bulk (macroscopic) complex conductivity as

$$\sigma_{\text{bulk}}^* = \sigma_0 \left(1 + \frac{m}{1 - m} \left(1 - \frac{1}{1 + (i\omega\tau)^c} \right) \right) \quad (6)$$

where σ_0 , m , τ and c are the macroscopic Cole–Cole parameters, the Cole–Cole exponent c being comprised between 0 and 1.

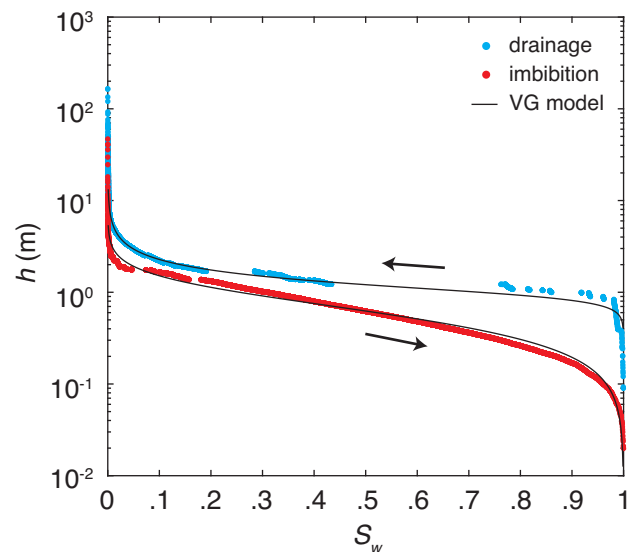


Figure 6. Representation of the matric potential h in function of the saturation S_w . The hysteretic behaviour is well evidenced. Note that during drainage, the sudden connection of tube clusters triggers significant jumps in the saturation state. The black lines correspond to the Van Genuchten model obtained from independent fitting of the drainage and imbibition data (see Table 1).

3 RESULTS

3.1 Relative permeability, resistivity index and characteristic lengths

The matric potential h (computed using eq. 2 for all radii) as a function of the saturation S_w exhibits a hysteretic behaviour (Fig. 6) as observed in real media (e.g. Mualem 1973; Pham *et al.* 2005). Hysteresis is also observed for the relative permeability (Fig. 7a), even

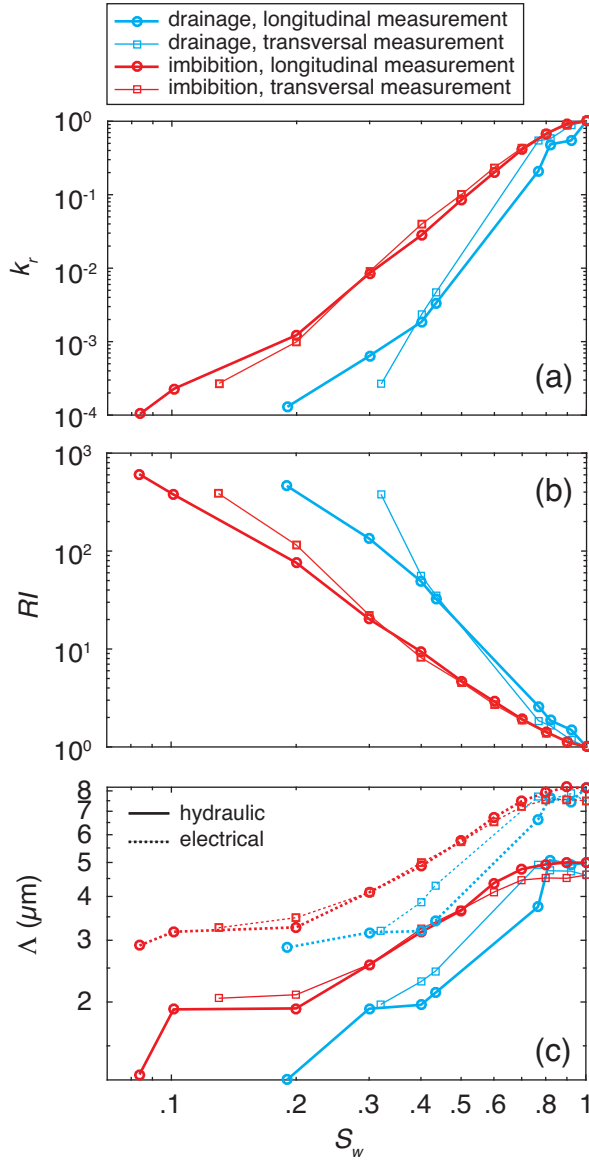


Figure 7. Evolution of the relative permeability k_r (a), of the resistivity index RI (b) and of the hydraulic and electrical characteristic lengths Λ_h and Λ_e (c) as a function of the saturation of the network. All quantities behave hysteretically, except the relative permeability in the transversal direction (i.e. between nodes $x = 1$ and $x = N_x$, see Fig. 1).

though the hysteretic behaviour is less marked when the relative permeability is measured in the transversal direction. The relative permeability decreases with saturation, with the values computed during imbibition always larger than during drainage. Concerning the resistivity index (Fig. 7b), it increases with decreasing saturation, with the values computed during drainage larger than during imbibition. Moreover the measurements in the transversal and longitudinal direction are relatively close one to each other for saturation below 0.3. The hysteretic behaviour of the resistivity index computed along the longitudinal direction is very similar to those of the resistivity measurements reported by Knight (1991) for sandstone samples. We also observe a hysteretic behaviour of the characteristic lengths (Fig. 7c). Interestingly, the relationship between the characteristic lengths and the relative permeability seem to have two regimes (Fig. 8): for relative permeabilities lower than 0.002, the characteristic lengths do not vary with k_r ; for larger values, we

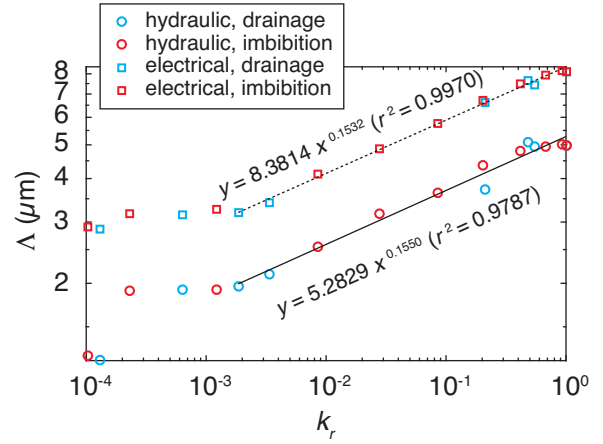


Figure 8. Evolution of the hydraulic and electrical characteristic lengths Λ_h and Λ_e in function of the relative permeability k_r .

can observe a power-law relationship $\Lambda = \Lambda(S_w = 1)k_r^\beta$ with an exponent β around 0.154.

3.2 SIP spectra

We observe a marked decrease of the amplitude of the complex resistivity during drainage, in both longitudinal and transversal directions (Figs 9a and c). With decreasing saturation, the phase spectrum tends to sharpen; its peak frequency (i.e. the frequency associated with the maximum value of the phase) moves towards higher frequencies, and its amplitude increases (Figs 9b and d). During imbibition (Fig. 10), the spectra follow the opposite behaviour, that is, an increase for the amplitude of the complex resistivity, a broadening of the phase curve, with a decrease of the peak frequency and a decrease of the phase amplitude.

All the SIP curves can be fitted by a Pelton model in conductivity (eq. 6), with very good fit. It is thus possible to draw the evolution of the model parameters with saturation, that is, the DC conductivity σ_0 (Fig. 11a), the chargeability m (Fig. 11b), the decimal logarithm of the time constant τ (Fig. 11c) and the Cole–Cole exponent c (Fig. 11d). All of them exhibit a hysteretic behaviour with respect to the saturation, in both longitudinal and transversal direction, even though it is less marked for the Cole–Cole exponent.

4 DISCUSSION

4.1 Hydrodynamic

Concerning the evolution of the matric potential, we fit these two curves using van Genuchten's (1980) model (Fig. 6):

$$h = -\frac{1}{\alpha} \left[\left(S_w^{-\frac{1}{n_{VG}}} \right) - 1 \right]^{\frac{1}{n_{VG}}} \quad (7)$$

Note that, in order to be able to fit the imbibition curve, it was necessary to decouple the two textural parameters as $m_{VG} \neq 1 - n_{VG}^{-1}$. In order to be consistent we optimized the three parameters α (in m^{-1}), m_{VG} , n_{VG} for both the drainage and imbibition curves, the best fit parameters are presented in Table 1. As expected from the literature, at a given saturation, the matric potential obtained during the drainage is higher than the one during the imbibition (e.g. Mualem 1984, his fig. 1). This results in a lower value of the

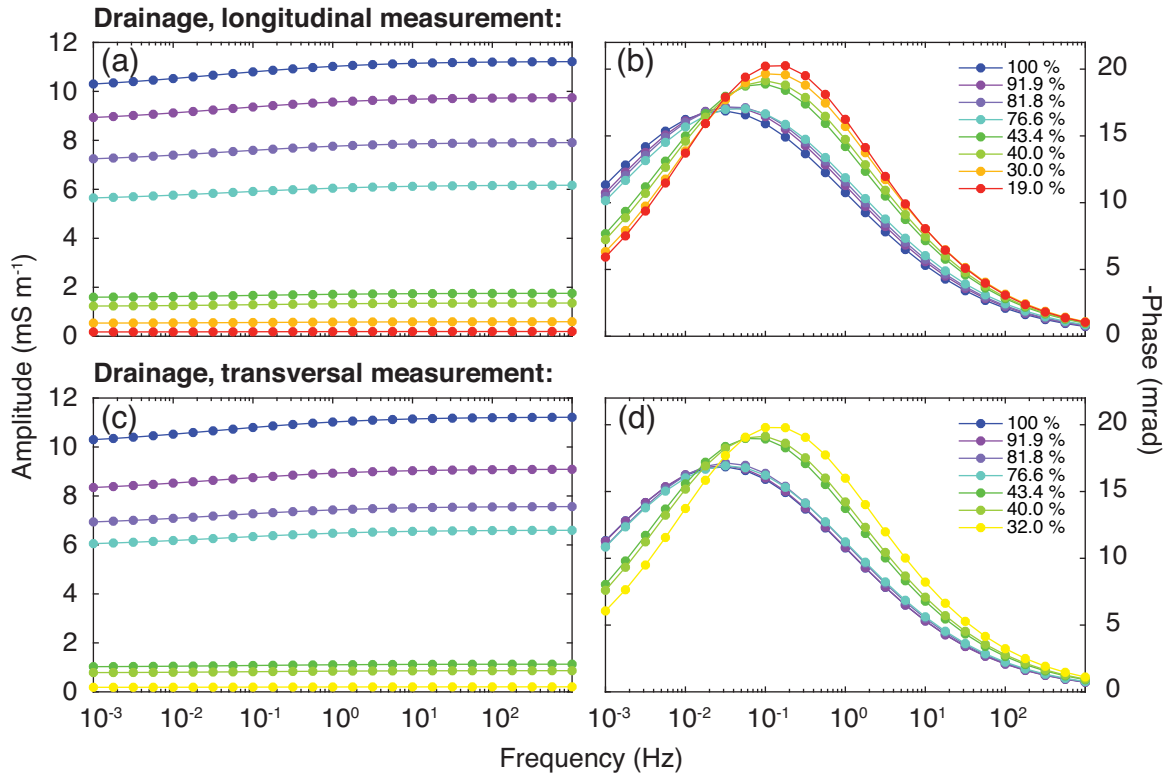


Figure 9. Complex conductivity spectra (amplitude and phase) at different states of saturation for the drainage, measured (a,b) in the longitudinal direction (i.e. between nodes $y = 1$ and $y = N_y$ and (c,d) in the transversal direction (i.e. between nodes $x = 1$ and $x = N_x$). Note the decrease in amplitude spectra, and the increase of the frequency peak in the phase spectra with decreasing saturation.

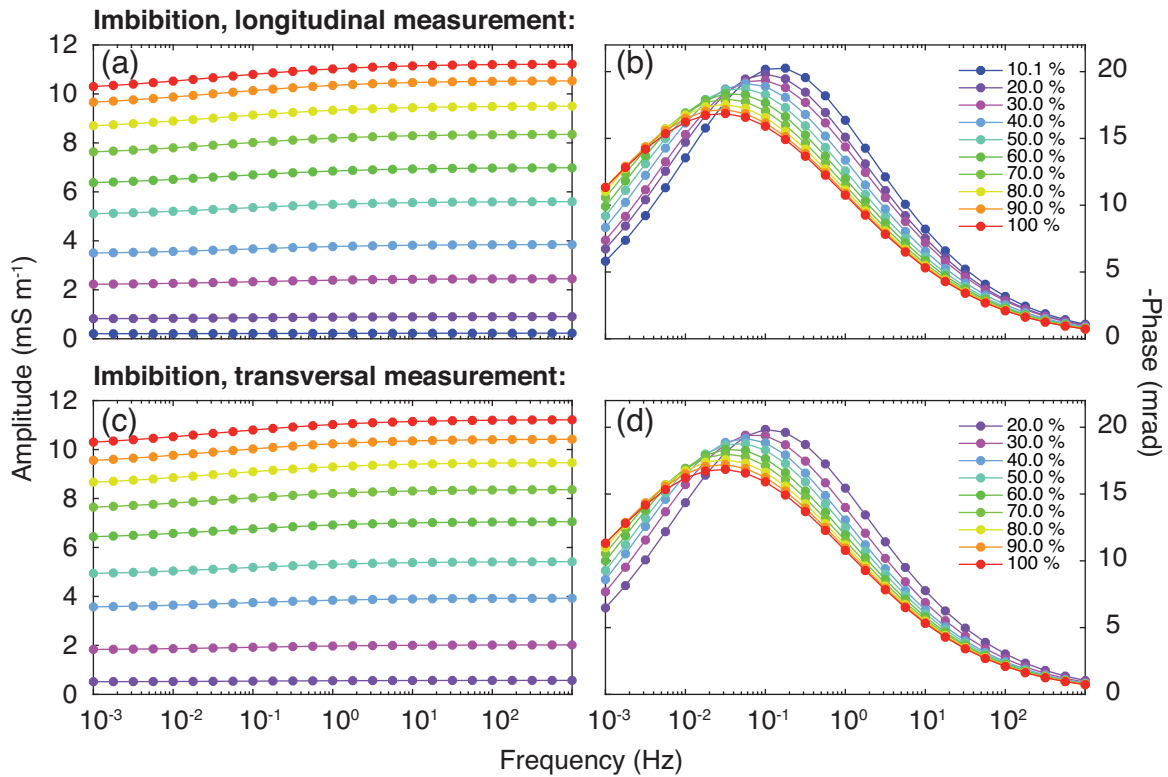


Figure 10. Complex conductivity spectra (amplitude and phase) at different states of saturation for the imbibition, measured (a,b) in the longitudinal direction (i.e. between nodes $y = 1$ and $y = N_y$ and (c,d) in the transversal direction (i.e. between nodes $x = 1$ and $x = N_x$). Note the increase in amplitude spectra, and the decrease of the frequency peak in the phase spectra with increasing saturation.

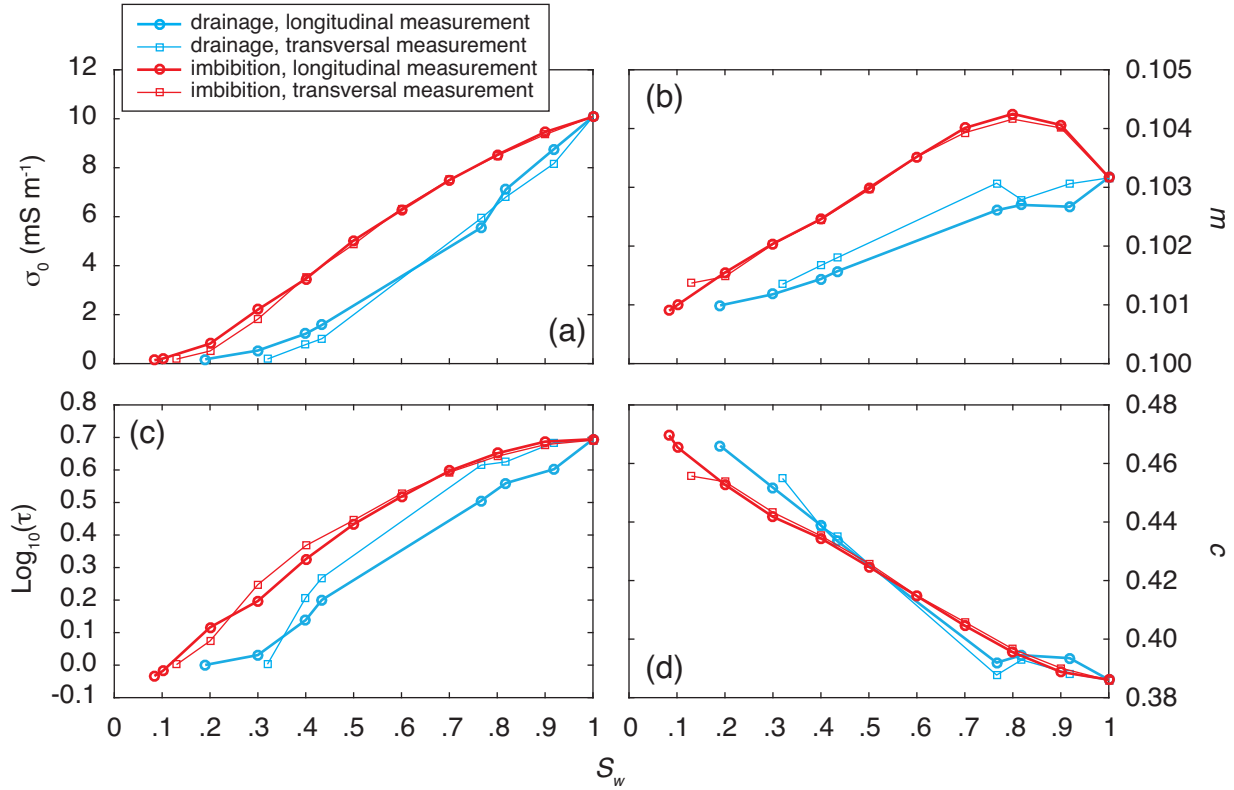


Figure 11. Evolution of the macroscopic Cole–Cole parameters: (a) DC conductivity σ_0 , (b) chargeability m , (c) time constant τ and (d) Cole–Cole exponent c in function of the saturation S_w , obtained by fitting the macroscopic complex resistivity spectra (Figs 9 and 10). All parameters exhibit a hysteretic behaviour, even though it is less clear for c .

Table 1. Best fit values obtained for the Van Genuchten model displayed in Fig. 6. The Root Mean Square Error is computed using

$$\text{RMSE} = \sqrt{\frac{1}{N} \sum_{i=1}^N [\log_{10}(h_i^{\text{predicted}}) - \log_{10}(h_i^{\text{measured}})]^2}.$$

Model parameter	Drainage	Imbibition
α (m)	1.048	0.768
m_{VG} (–)	0.373	2.769
n_{VG} (–)	7.083	1.7141
RMSE* (m)	0.0709	0.0832

optimized α parameter for the imbibition curve than for the drainage one (Table 1).

The resistivity index denotes the ratio between the resistivity at full saturation divided by the resistivity at a given saturation S_w . We model the evolution of the resistivity index using second Archie’s law (1942) neglecting in the present study the effect of surface conductivity. This yields:

$$\text{RI} = \frac{1}{S_w^n}. \quad (8)$$

We find that the saturation exponent n is equal to 4 for drainage and to 2.5 for imbibition (Fig. 12a). Although $n = 4$ is fairly high and surprising for a natural porous medium (generally expected around 2 ± 0.5 in water wet rocks, see Archie 1942 or Glover 2015), it could be linked to electrical tortuosity in 2-D media. Indeed, Jougnot *et al.* (2016) obtained the same value while monitoring the electrical conductivity of a 2-D synthetic medium submitted to various drainage procedures.

We observe a hysteresis in the relative permeability (Fig. 7a). This is apparently in contradiction with models, which predict that

the $k_r(S_w)$ is non-hysteretic (e.g. Soldi *et al.* 2017), and with measurements (e.g. Topp & Miller 1966; Van Genuchten 1980; Mualem 1986). However, for saturations above 40 per cent, simulations show that the transversal section available for transport is more reduced during drainage than during imbibition (Fig. 13, for saturation of 80 per cent), making the permeability also more reduced during drainage. In other words, since the geometry of the desaturated clusters are very different during drainage and imbibition, the flow paths are not similar, and so the resulting permeability. Note here that we were not able to fit the relative permeability curve versus saturation with classical models (in particular Brooks & Corey 1964; van Genuchten 1980). The only very good fit was obtained for the longitudinal drainage (for both Brooks & Corey (1964) and van Genuchten (1980) models, see below). For the three other curves, the best fit models were not able to reproduce them for the saturation range comprised between 0.6 and 0.95, as the relative permeabilities do not follow the expected power-law function.

4.2 SIP spectra

The evolution of the SIP spectra with saturation (Figs 9 and 10) is very similar to those reported by Breede *et al.* (2011) and Breede (2012). Indeed, Breede *et al.* (2011) showed a decrease of the conductivity amplitude spectra with decreasing saturation for unconsolidated sand with negligible surface conductivity (around $5 \mu\text{S cm}^{-1}$). Titov *et al.* (2004) also reported such a behaviour. Breede *et al.* (2011) and Breede (2012) also reported that the peak frequency slightly increased, the spectra are sharpened, and the maximum value of the phase increased with decreasing saturation. Also, on sandstone samples, Ulrich & Slater (2004) reported an increase

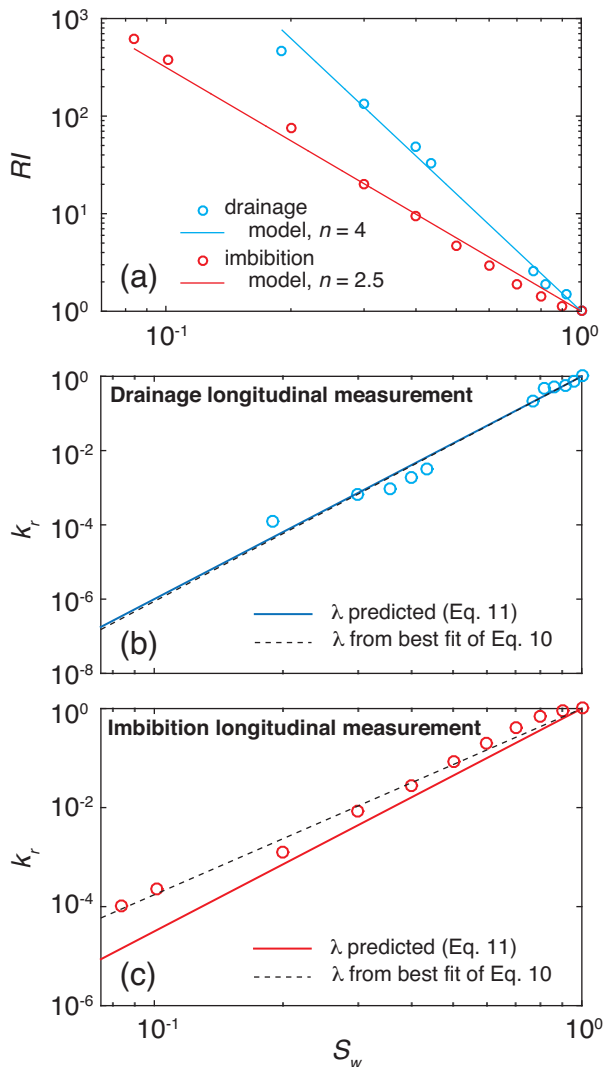


Figure 12. (a) Modelling of the resistivity index RI using $RI = S_w^{-n}$ for longitudinal measurements. The saturation exponent is equal to 4 for drainage and 2.5 for imbibition. Prediction of relative permeability k_r with Brooks & Corey (1964) model (eq. 10) using λ value determined using eq. (11) (continuous lines), and from best fit of eq. 10 (dotted lines), for (b) drainage and (c) imbibition.

of the phase at 1 Hz with decreasing saturation during drainage, and a decrease with increasing saturation during imbibition. Finally, Binley *et al.* (2005) observed an increase of the peak frequency with decreasing saturation on unsaturated consolidated sandstone samples. However, they did not observe a systematic increase in the maximum value of the phase, neither the sharpening of the spectra.

Concerning the Cole–Cole parameters, Titov *et al.* (2004) reported a decrease of the conductivity σ_0 with decreasing saturation for quartz–water–air mixtures, as we observe too (Fig. 11c). For the chargeability, Breede *et al.* (2011) reported a decrease with increasing saturation for sand. Also for sand, Titov *et al.* (2004) observed an increase of the chargeability for saturation increasing between 0 and 0.1 and a decrease for saturation increasing between 0.1 and 1. Revil *et al.* (2012) reported a similar behaviour, with an increase of the chargeability for saturation below 0.1 and a decrease for saturation above 0.1. In fact, this seems to be the opposite of what we get (Fig. 11b), in particular for drainage. For imbibition, we have such a behaviour, but with a change in slope at a saturation of 0.8, not

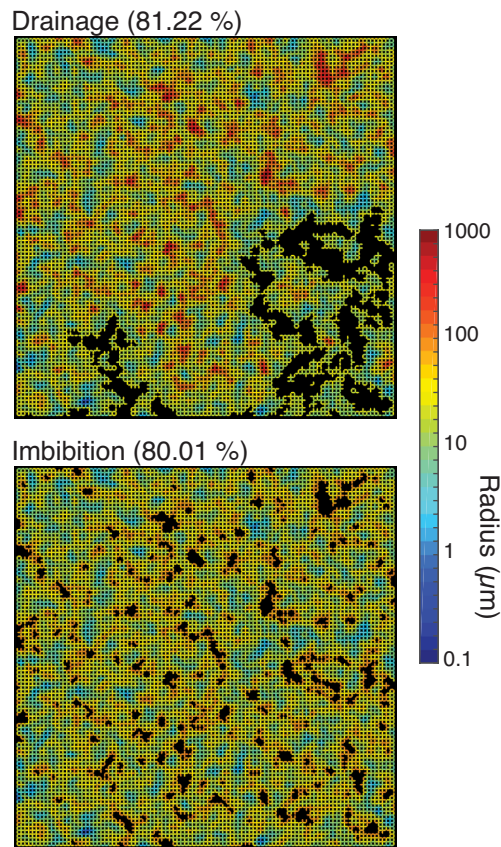


Figure 13. Network at about 80 per cent of saturation for (top) drainage and (bottom) imbibition.

0.1. Concerning the time constant τ , Breede *et al.* (2011), as well as Revil *et al.* (2012) observed an increase of the time constant τ with increasing saturation, as we do (Fig. 11c).

4.3 Link between SIP response and saturation and permeability

Revil *et al.* (2014a) proposed new relationships to relate directly the electrical conductivity as a function of the saturation to relative permeability $k_r(S_w)$ through the use of the characteristic length Λ . They suggested that $\Lambda(S_w) = \Lambda(S_w = 1) S_w$, which yield to his model A:

$$k_r = S_w^{2+n}, \quad (9)$$

where n is the saturation exponent as defined by Archie (1942; eq. 8). By comparing eq. (9) to the Brooks & Corey (1964) model:

$$k_r(S_w) = S_w^{\frac{2}{\lambda}+3}, \quad (10)$$

where λ is a textural parameter. Combining eqs (9) and (10) yields:

$$\lambda = \frac{2}{n-1}, \quad (11)$$

hence relating directly electrical (n) and hydraulic (λ) petrophysical parameters. By applying this to our data, where the saturation exponent n is equal to 4 and 2.5 for the drainage and imbibition respectively, gives λ equal to 0.667 and 1.333. Comparison between these predictions and best fit λ values (from eq. 10, $\lambda = 0.653$ and 2.633, respectively) are plotted on Figs 12(b) and (c) and reported in Table 2. Overall, these predictions of relative permeability

Table 2. Predicted and best fit values to describe the relative permeability function using eqs (10) and (11).

	Saturation exponent, n	Predicted λ	Best fit λ
Drainage	4	0.667	0.653
Imbibition	2.5	1.333	2.633

curve from electrical conductivity measurements are fairly good but would need to be checked on other realizations of synthetic porous media.

The relationship between the Cole–Cole DC conductivity σ_0 and the relative permeability appears to be a power law, with an early regime ($k_r < 0.01$) and a late one, for both drainage and imbibition (Fig. 14a). A similar behaviour was reported by Breede (2012) on SIP measurements on pure sand and sand–clay mixtures. For the imbibition and longitudinal measurements, we obtain the relations $\sigma_0 = 52.056 k_r^{0.6472}$ in the early regime, and $\sigma_0 = 9.9404 k_r^{0.3039}$ in the late one (Fig. 14b). Concerning the evolution of the time constant τ with respect to k_r , it is also a power law (Fig. 14c), but it seems that there is only one regime, except for the imbibition with measurements in the longitudinal direction (Fig. 14d). In this case, we find $\tau = 2.9498 k_r^{0.1283}$ in the early regime, and $\tau = 4.9139 k_r^{0.2392}$. This behaviour is very similar to what Breede (2012) measured (see her fig. 4.8): she obtained exponents in of the same order of magnitude (between 0.07 and 0.18). Finally, Binley *et al.* (2005) also reported a linear relationship between the time constant and the longitudinal hydraulic conductivity measured on sandstone samples, with exponent of 0.26 (their fig. 11).

The Cole–Cole exponent c seems to decrease linearly with increasing saturation (Fig. 15), meaning that the value of c may be a proxy for the saturation state, even though the coefficient of the

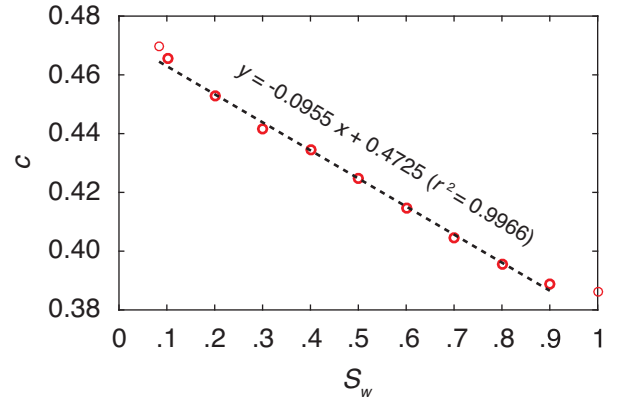


Figure 15. Evolution of the Cole–Cole exponent c in function of the saturation S_w during imbibition (longitudinal measurement). The relation is quasi linear, meaning that the saturation state could be deduced from c , even though the slope is rather small.

slope is weak. One can notice that when decreasing saturation, the width of the radius distribution becomes narrower, that is, less heterogeneous. Therefore the macroscopic value of c tends towards the local value of c_l , a behaviour also reported by Mainault *et al.* (2017).

The characteristic lengths Λ_h and Λ_e decrease with increasing peak frequency f_{peak} (the frequency for which the amplitude of the SIP phase spectrum is maximal), that is, with decreasing saturation (Fig. 16). The relationship between these quantities seems to be power laws, with an exponent of about -0.68 . More interestingly, the peak frequency is related to the relative permeability also by a power law with an exponent of -0.185 (Fig. 17). It means that SIP

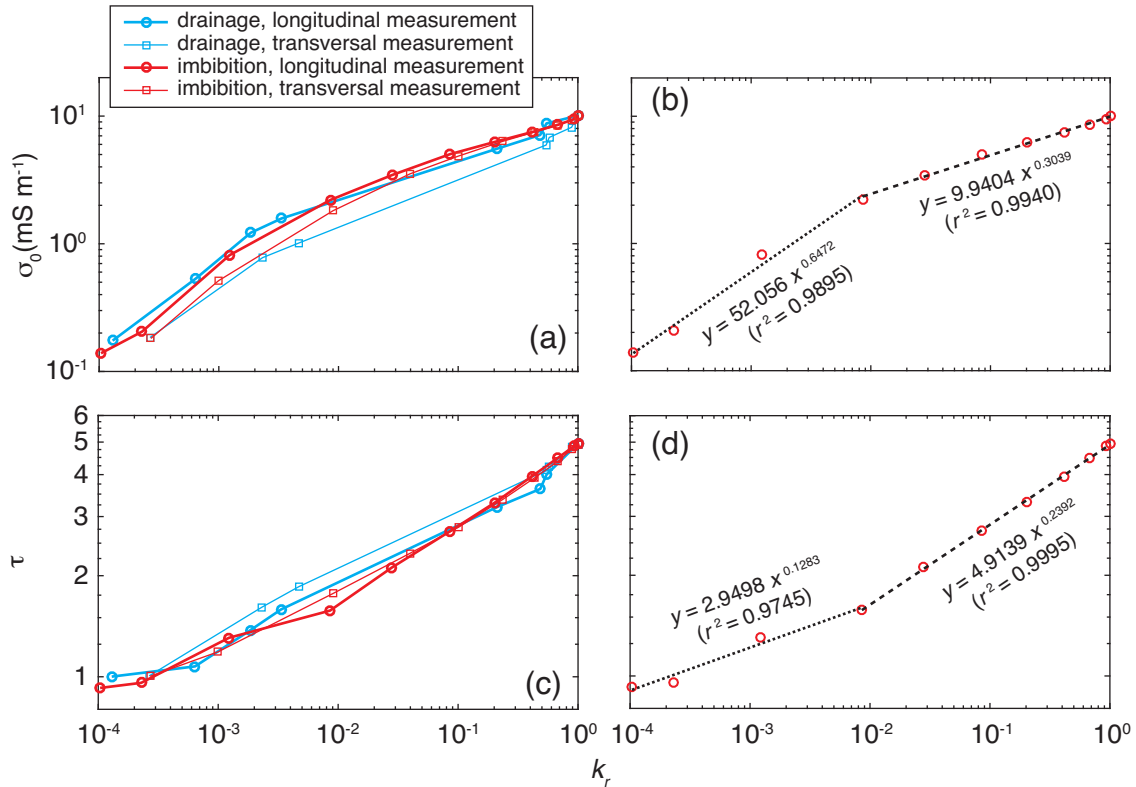


Figure 14. Evolution of the (a,b) DC conductivity σ_0 and (c,d) time constant τ in function of the relative permeability k_r . In (b) and (d), only data for longitudinal measurements during imbibition are considered.

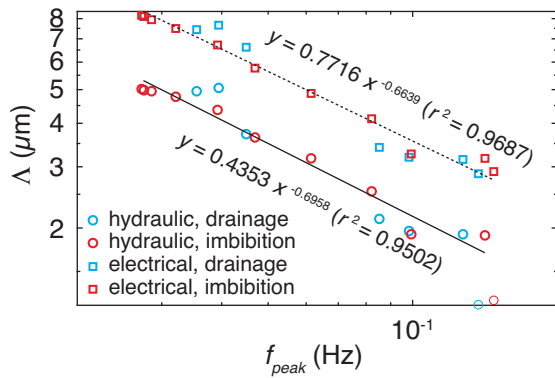


Figure 16. Evolution of the characteristic hydraulic and electrical lengths Δ_h and Δ_e in function of the peak frequency f_{peak} , for longitudinal measurements.

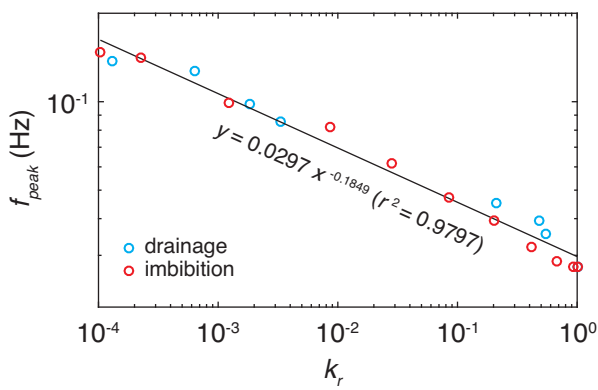


Figure 17. Evolution of the peak frequency f_{peak} in function of the relative permeability k_r (longitudinal measurements).

measurements could give access directly to the relative permeability, or, at least, that measured variations of the peak frequency due to saturation changes can provide information about the associated variations of the relative permeability.

Obviously, only one simulation is not sufficient to draw general conclusions. That is the reason why we carried out similar calculations on four supplementary networks. In all cases, the behaviour of the relative permeability, the resistivity index and the characteristic lengths in function of the saturation was similar to the behaviour observed on the primary network (Fig. 7). The complex conductivity spectra (Figs 9 and 10) were also similar, as well as the behaviour of the Cole–Cole parameters in function of the saturation (Fig. 11). Concerning the relationships between the DC conductivity and the relative permeability, the previously described trend (Figs 14a and b) is confirmed, with two power-law regimes (Fig. 18a). Similarly, for the relationships between the time constant and the relative permeability, the previously described trend (Figs 14c and d) seems to be also verified by the five simulations (Fig. 18b). The linear trend between the Cole–Cole exponent and the saturation (Fig. 15) is also observed (Fig. 18c). Regarding the power-law relationship between the characteristic lengths and the relative permeability (Fig. 8), it seems that in the general case it extends to the whole range of relative permeability (Fig. 19a). Finally, the power-law regime between the characteristic lengths and the peak-frequency (Fig. 16) can be generalized (Fig. 19b), as well as the power-law regime between the peak frequency and the relative permeability (Figs 17 and 19c).

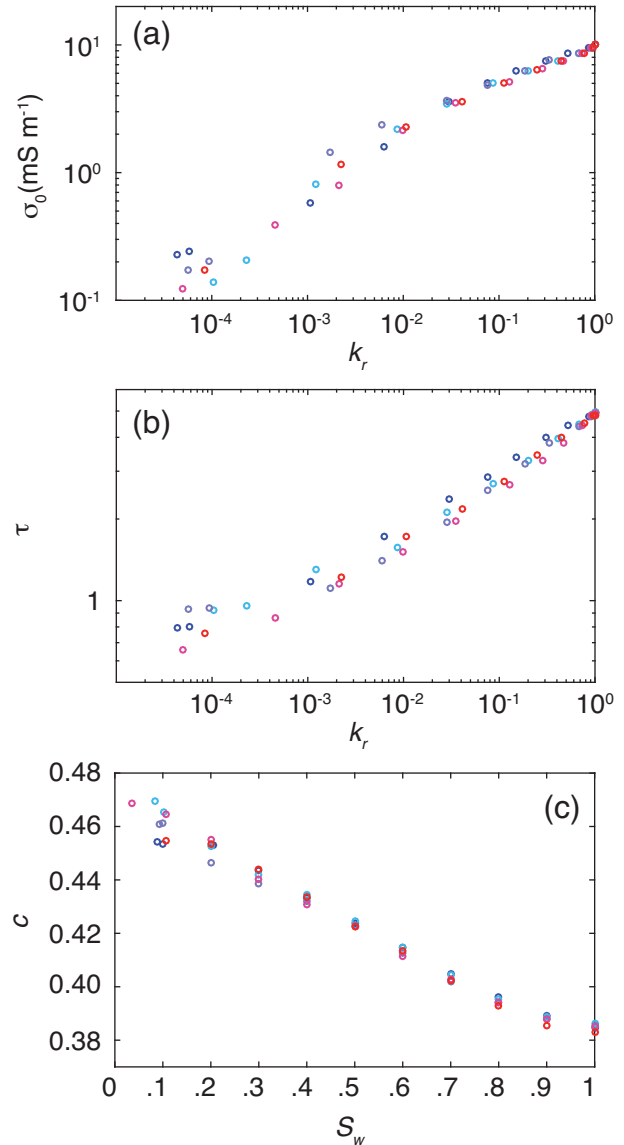


Figure 18. Results from five network simulations during imbibition. Evolution of the (a) DC conductivity σ_0 and (b) time constant τ in function of the relative permeability k_r , and (c) evolution of the Cole–Cole exponent c in function of the saturation S_w .

Even though the representation of a porous medium by a correlated 2-D square network is a very strong approximation, the simulations that we performed reproduced some behaviours previously reported by Breede (2012) on sands for instance, in particular the evolution of the DC conductivity and the time constant with the relative permeability. They also showed the potential interest of SIP measurements during drainage and imbibition to estimate some hydraulic parameters such as relative permeability from SIP parameters (in particular the peak frequency). Further works imply the extension of the method to 3-D networks, for which the saturation and desaturation pathways should be somehow different, and also to test other types of mesh, since the transport properties of a network can depend on its topology (e.g. Bernabé *et al.* 2003). Finally, an experimental validation of the relationships that we deduced is highly advisable.

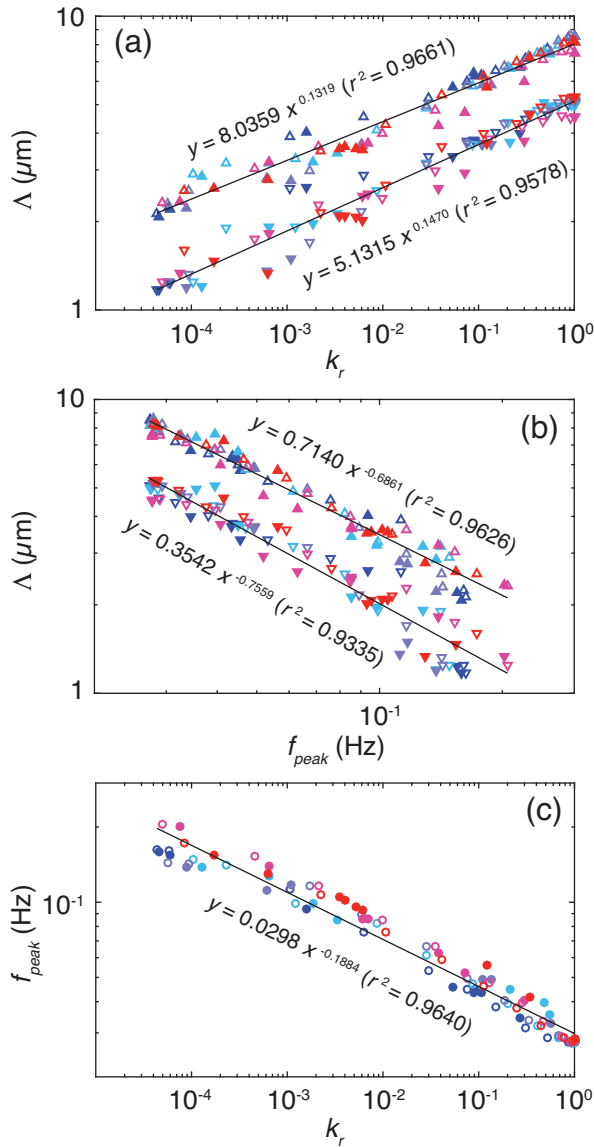


Figure 19. Results from five network simulations: evolution of the characteristic lengths Λ_h and Λ_e in function of (a) the relative permeability k_r and (b) the peak frequency f_{peak} , and evolution of the frequency peak f_{peak} in function of the relative permeability k_r . (c) ∇ : Λ_h , \blacktriangle : Λ_e , plain symbols correspond to drainage and open symbols to imbibition.

5 CONCLUSIONS

We are able to simulate saturation and desaturation processes in 2-D square networks, and to calculate the associated resistivity index, relative permeability, characteristic lengths and SIP spectra (under the assumption that the parameters $\sigma_{0,l}$, m_l and D_l are the same for all tubes, as done by Maïneult *et al.* (2017), and that the surface conductivity can be neglected). The behaviour of SIP spectra is globally in agreement with what was previously reported in the literature. In particular, for the phase spectra, there is an increase of the peak frequency with decreasing saturation. We also evidenced that the resistivity index, the relative permeability, the characteristic lengths and the macroscopic Cole–Cole parameters, except the Cole–Cole exponent c , present a hysteretic behaviour. We also show that the frequency peak is directly related to the characteristic lengths and to the relative permeability, meaning that permeability should be accessible from SIP phase spectra. As reported in the literature, we

observe that the DC conductivity σ_0 and the time constant τ are related to the apparent permeability with a power law, meaning, here again, that quantitative information about the permeability can be deduced from Cole–Cole parameters. Finally, the Cole–Cole exponent is a quasi linear function of saturation. The computational exercise that we performed therefore evidences the interest of the SIP method for the study of the non-saturated medium and their evolution with water saturation. Further works implies the extension to 3-D networks, the trapping of water in desaturated pores to account for the residual, irreducible saturation, as well as including the surface conductivity in the model.

ACKNOWLEDGEMENTS

The authors sincerely thank the reviewers and the associate editor for their helpful comments.

REFERENCES

- Archie, G., 1942. The electrical resistivity log as an aid in determining some reservoir characteristics, *Trans. Am. Inst. Min. Metall. Eng.*, **146**, 54–61.
- Attwa, M. & Günther, T., 2013. Spectral induced polarization measurements for predicting the hydraulic conductivity in sandy aquifers, *Hydrol. Earth Syst. Sci.*, **17**, 4079–4094.
- Avellaneda, M. & Torquato, S., 1991. Rigorous link between fluid permeability, electrical conductivity, and relaxation times for transport in porous media, *Phys. Fluids A*, **3**, 2529–2540.
- Bear, J., 1972. *Dynamics of Fluids in Porous Media*, Elsevier.
- Berg, S. *et al.*, 2013. Real-time 3D imaging of Haines jumps in porous media flow, *Proc. Natl. Acad. Sci. USA*, **110**(10), 3755–3759.
- Bernabé, Y., 1995. The transport properties of networks of cracks and pores, *J. geophys. Res.*, **100**(B3), 4231–4241.
- Bernabé, Y. & Revil, A., 1995. Pore-scale heterogeneity, energy dissipation and the transport properties of rocks, *Geophys. Res. Lett.*, **22**(12), 1529–1532.
- Bernabé, Y., Bruderer-Weng, C. & Maïneult, A., 2003. Permeability fluctuations in heterogeneous networks with different dimensionality and topology, *J. geophys. Res.*, **108**(B7), 2351, doi:10.1029/2002JB002326.
- Binley, A. & Kemna, A., 2005. DC resistivity and induced polarization methods, in *Hydrogeophysics*, pp. 129–156, eds Rubin, Y. & Hubbard, S.S., Springer.
- Binley, A., Slater, L.D., Fukes, M. & Cassiani, G., 2005. Relationship between spectral induced polarization and hydraulic properties of saturated and unsaturated sandstones, *Water Resour. Res.*, **41**, W12417, doi:10.1029/2005WR004202.
- Binley, A., Hubbard, S.S., Huisman, J.A., Revil, A., Robinson, D.A., Singha, K. & Slater, L.D., 2015. The emergence of hydrogeophysics for improved understanding of subsurface processes over multiple scales, *Water Resour. Res.*, **51**(6), 3837–3866.
- Breede, K., 2012. Characterization of effective hydraulic properties of unsaturated porous media using spectral induced polarization (SIP), *PhD thesis*, Bonn University.
- Breede, K., Kemna, A., Esser, O., Zimmermann, E., Vereecken, H. & Huisman, J.A., 2011. Joint measurement setup for determining spectral induced polarization and soil hydraulic properties, *Vadose Zone J.*, **10**, 716–726.
- Brooks, R.H. & Corey, A.T., 1964. *Hydraulic Properties of Porous Media*, vol. 3 of Hydrology Papers, Colorado State University.
- Cosenza, P., Ghorbani, A., Florsch, N. & Revil, A., 2007. Effects of drying on the low-frequency electrical properties of Tournemire argillites, *Pure appl. Geophys.*, **164**(10), 2043–2066.
- David, C., 1993. Geometry of flow paths for fluid transport in rocks, *J. geophys. Res.*, **98**(B7), 12 267–12 278.

- David, C., Guéguen, Y. & Pampoukis, G., 1990. Effective medium theory and network theory applied to the transport properties of rock, *J. geophys. Res.*, **95**(B5), 6993–7005.
- DiCarlo, D.A., Cidoncha, J.I.G & Hickey, C., 2003. Acoustic measurements of pore-scale displacements, *Geophys. Res. Lett.*, **30**(17), 1901, doi:10.1029/2003GL017811.
- Doussan, C. & Ruy, S., 2009. Prediction of unsaturated soil hydraulic conductivity with electrical conductivity, *Water Resour. Res.*, **45**, W10408, doi:10.1029/2008WR007309.
- Glover, P.W.J., 2015. Geophysical properties of the near surface earth: electrical properties, in *Resources in the Near-Surface Earth, Treatise on Geophysics*, 2nd edn, Vol. 11, pp. 89–137, eds Slater, L. & Schubert, G., Elsevier.
- Guarracino, L., 2007. Estimation of saturated hydraulic conductivity K_s from the van Genuchten shape parameter α , *Water Resour. Res.*, **43**, W11502, doi:10.1029/2006WR005766.
- Haas, A. & Revil, A., 2009. Electrical burst signature of pore-scale displacements, *Water Resour. Res.*, **45**, W10202, doi:10.1029/2009WR008160.
- Haines, W.B., 1930. Studies in the physical properties of soils. V. The hysteresis effect in capillary properties, and the modes of water distribution associated therewith, *J. Agric. Sci.*, **20**(1), 97–116.
- Hördt, A., Blaschek, R., Kemna, A. & Zisser, N., 2007. Hydraulic conductivity estimation from induced polarization data at the field scale—the Krauthausen case history, *J. Appl. Geophys.*, **62**, 33–46.
- Hubbard, S.S. & Linde, N., 2011. Hydrogeophysics, in *Treatise on Water Science*, Vol. 2, pp. 401–434, ed. Wilderer, P., Academic Press.
- Johnson, D.L., Koplik, J. & Schwartz, L.M., 1986. New pore-size parameter characterizing transport in porous media, *Phys. Rev. Lett.*, **57**(20), 2564–2567.
- Johnson, T.C., Versteeg, R.J., Ward, A., Day-Lewis, F.D. & Revil, A., 2010. Improved hydrogeophysical characterization and monitoring through high performance electrical geophysical modeling and inversion, *Geophysics*, **75**(4), WA27–WA41.
- Jougnot, D., Ghorbani, A., Revil, A., Leroy, P. & Cosenza, P., 2010. Spectral induced polarization of partially saturated clay-rocks: A mechanistic approach, *Geophys. J. Int.*, **180**(1), 210–224.
- Jougnot, D., Linde, N., Revil, A. & Doussan, C., 2012. Derivation of soil-specific streaming potential electrical parameters from hydrodynamic characteristics of partially saturated soils, *Vadose Zone J.*, **11**, doi:10.2136/vzj2011.0086.
- Jougnot, D., Jimenez-Martinez, J., Meheust, Y., Le Borgne, T. & Linde, N., 2016. Electrical resistivity monitoring of saline tracer fingering under partially saturated conditions: a pore-scale fluorimetry study, in *22nd European Meeting of Environmental and Engineering Geophysics, EAGE Near Surface Geoscience*, Barcelona, Spain, September 5–8, doi:10.3997/2214-4609.201601953.
- Jurin, J., 1717. An account of some experiments shown before the Royal Society; with an enquiry into the cause of the ascent and suspension of water in capillary tubes, *Philos. Trans.*, **30**(351–363), 739–747.
- Jury, W.A., Gardner, W.R. & Gardner, W.H. 1991. *Soil Physics*, John Wiley and Sons.
- Kirchhoff, G., 1845. Ueber den Durchgang eines elektrischen Stromes durch eine Ebene, insbesondere durch eine kreisförmige, *Ann. Phys.*, **140**(4), 497–514.
- Kirkpatrick, S., 1973. Percolation and conduction, *Rev. Modern Phys.*, **45**, 574–588.
- Knight, R., 1991. Hysteresis in the electrical resistivity of partially saturated sandstones, *Geophysics*, **56**(12), 2139–2147.
- Koplik, J., 1981. On the effective medium theory of random linear networks, *J. Phys. C: Solid State Phys.*, **14**, 4821–4837.
- Maineult, A., Revil, A., Camerlynck, C., Florsch, N. & Titov, K. 2017. Upscaling of spectral induced polarization response using random tube networks, *Geophys. J. Int.*, **209**(2), 948–960.
- Mualem, Y., 1973. Modified approach to capillary hysteresis based on a similarity hypothesis, *Water Resour. Res.*, **9**(5), 1324–1331.
- Mualem, Y., 1984. A modified dependent-domain theory of hysteresis, *Soil Sci.*, **137**(5), 283–291.
- Mualem, Y., 1986. Hydraulic conductivity of unsaturated soils: prediction and formulas, in *Methods of Soil Analysis: Part 1 – Physical and Mineralogical Methods*, Vol. 5, pp. 799–823, ed. Klute, A., Soil Science Society of America.
- Niu, Q. & Revil, A., 2016. Connecting complex conductivity spectra to mercury porosimetry of sedimentary rocks, *Geophysics*, **81**(1), E17–E32.
- Niu, Q., Fratt, D. & Wang, Y.-H., 2015. The use of electrical conductivity measurements in the prediction of hydraulic conductivity of unsaturated soils, *J. Hydrol.*, **522**, 475–487.
- Or, D. & Tuller, M., 1999. Liquid retention and interfacial area in variably saturated porous media. Upscaling from single-pore to sample-scale model, *Water Resour. Res.*, **35**(12), 3591–3605.
- Packard, R.G., 1953. Streaming potentials across glass capillaries for sinusoidal pressure, *J. Chem. Phys.*, **21**(2), 303–307.
- Pham, H.Q., Fredlund, D.G. & Barbour, S.L., 2005. A study of hysteresis models for soil-water characteristic curves, *Can. Geotech. J.*, **42**, 1548–1568.
- Revil, A., Koch, K. & Holliger, K., 2012. Is it the grain size or the characteristic pore size that controls the induced polarization relaxation time of clean sands and sandstones?, *Water Resour. Res.*, **48**, W05602, doi:10.1029/2011WR011561.
- Revil, A., Bernier, G., Karaoulis, M., Sava, P., Jardani, A. & Kulesa, B., 2014a. Seismoelectric coupling in unsaturated porous media: theory, petrophysics, and saturation front localization using an electroacoustic approach, *Geophys. J. Int.*, **196**(2), 867–884.
- Revil, A., Florsch, N. & Camerlynck, C., 2014b. Spectral induced polarization porosimetry, *Geophys. J. Int.*, **198**(2), 1016–1033.
- Revil, A., Binley, A., Mejus, L. & Kessouri, P., 2015. Predicting permeability from the characteristic relaxation time and intrinsic formation factor of complex conductivity spectra, *Water Resour. Res.*, **51**(8), 6672–6700.
- Schmutz, M., Blondel, A. & Revil, A., 2012. Saturation dependence of the quadrature conductivity of oil-bearing sands, *Geophys. Res. Lett.*, **39**, L03402, doi:10.1029/2011GL050474.
- Schwartz, L.M., Sen, P.N. & Johnson, D.L., 1989. Influence of rough surfaces on electrolytic conduction in porous media, *Phys. Rev. B*, **40**(4), 2450–2458.
- Sen, P.N., Scala, C. & Cohen, M. H., 1981. Self-similar model for sedimentary rocks with application to the dielectric constant of fused glass beads, *Geophysics*, **46**(5), 781–795.
- Shainberg, I., Rhoades, J.D. & Prather, R.J., 1980. Effect of exchangeable sodium percentage, cation exchange capacity, and soil solution concentration on soil electrical conductivity, *Soil Sci. Soc. Am. J.*, **44**, 469–473.
- Slater, L. & Lesmes, D.P., 2002. Electrical-hydraulic relationships observed for unconsolidated sediments, *Water Resour. Res.*, **38**(10), 1213, doi:10.1029/2001WR001075.
- Slater, L., Barrash, W., Montrey, J. & Binley, A., 2014. Electrical-hydraulic relationships observed for unconsolidated sediments in the presence of a cobble framework, *Water Resour. Res.*, **50**, 5721–5742.
- Soldi, M., Guarracino, L. & Jougnot, D., 2017. A simple hysteretic constitutive model for unsaturated flow, *Transp. Porous Media*, **120**, 271–285.
- Soueid Ahmed, A., Jardani, A., Revil, A. & Dupont, J.-P., 2016a. Specific storage and hydraulic conductivity tomography through the joint inversion of hydraulic heads and self-potential data, *Adv. Water Resour.*, **89**, 80–90.
- Soueid Ahmed, A., Jardani, A., Revil, A. & Dupont, J.-P., 2016b. Joint inversion of hydraulic head and self-potential data associated with harmonic pumping tests, *Water Resour. Res.*, **52**(9), 6769–6791.
- Tarasov, A. & Titov, K., 2013. On the use of the Cole–Cole equations in spectral induced polarization, *Geophys. J. Int.*, **195**(1), 352–356.
- Titov, K., Kemna, A., Tarasov, A. & Vereecken, H., 2004. Induced polarization of unsaturated sands determined through time domain measurements, *Vadose Zone J.*, **3**(4), 1160–1168.
- Tong, M., Wang, W., Li, L., Jiang, Y. & Shi, D., 2004. Estimation of permeability of shaly sand reservoir from induced polarization relaxation time spectra, *J. Petrol. Sci. Eng.*, **45**, 31–40.
- Topp, G.C. & Miller, E.E., 1966. Hysteretic moisture characteristics and hydraulic conductivities for glass-bead media, *Soil Sci. Soc. Am. J.*, **30**(2), 156–162.

- Turcotte, D.L., 1997. *Fractal and Chaos in Geophysics*, 2nd edn, Cambridge Univ. Press.
- Ulrich, C. & Slater, L.D., 2004. Induced polarization measurements on unsaturated, unconsolidated sands, *Geophysics*, **69**(3), 762–771.
- van Genuchten, M.T., 1980. A closed-form equation for predicting the hydraulic conductivity of unsaturated soils, *Soil Sci. Soc. Am. J.*, **44**, 892–898.
- Vereecken, H., Binley, A., Cassiani, G., Revil, A. & Titov, K., 2006. *Applied Hydrogeophysics*, Springer.
- Weller, A., Nordsiek, S. & Debschütz, W., 2010. Estimating permeability of sandstone samples by nuclear magnetic resonance and spectral-induced polarization, *Geophysics*, **75**(6), E215–E226.

APPENDIX: RELATIVE PERMEABILITY, RESISTIVITY INDEX AND CHARACTERISTIC LENGTHS

We consider the network, saturated or not. The hydraulic flux $F_{p \rightarrow q}$ through a tube linking two nodes p and q writes

$$F_{p \rightarrow q} = \frac{\pi r_{p \rightarrow q}^4}{8\eta} \frac{P_p - P_q}{l} = g_{p \rightarrow q}^h (P_p - P_q), \quad (\text{A1})$$

where $r_{p \rightarrow q}$ is the radius of the tube and l its length, $g_{p \rightarrow q}^h$ is the hydraulic conductance, η the dynamic viscosity, and P the hydraulic pressure. To eliminate the length l , we introduce the modified hydraulic flux $\Phi_{p \rightarrow q}^h$:

$$\Phi_{p \rightarrow q}^h = F_{p \rightarrow q} l = \frac{\pi r_{p \rightarrow q}^4}{8\eta} (P_p - P_q) = \gamma_{p \rightarrow q}^h (P_p - P_q). \quad (\text{A2})$$

Neglecting the surface conductivity, the electrical flux $J_{p \rightarrow q}$, taken writes:

$$J_{p \rightarrow q} = \sigma_w \pi r_{p \rightarrow q}^2 \frac{V_p - V_q}{l} = g_{p \rightarrow q}^e (V_p - V_q), \quad (\text{A3})$$

where σ_w is the electrical conductivity of the saturating fluid, V the electrical potential and g^e the electrical conductance. To eliminate l and the fluid conductivity σ_w , we use the modified electrical flux $\Phi_{p \rightarrow q}^e$:

$$\Phi_{p \rightarrow q}^e = J_{p \rightarrow q} \frac{l}{\sigma_w} = \pi r_{p \rightarrow q}^2 (V_p - V_q) = \gamma_{p \rightarrow q}^e (V_p - V_q). \quad (\text{A4})$$

At any node inside the square network (Fig. 1), Kirchhoff's law (1845) writes

$$Z_{x,y-1 \rightarrow x,y} + Z_{x-1,y \rightarrow x,y} + Z_{x+1,y \rightarrow x,y} + Z_{x,y+1 \rightarrow x,y} = 0, \quad (\text{A5})$$

with Z equal to F or J respectively. Using eq. (A1) or (A3), this leads to

$$\begin{aligned} & a_{x,y-1 \rightarrow x,y} X_{x,y-1} + a_{x-1,y \rightarrow x,y} X_{x-1,y} \\ & - (a_{x,y-1 \rightarrow x,y} + a_{x-1,y \rightarrow x,y} + a_{x+1,y \rightarrow x,y} + a_{x,y+1 \rightarrow x,y}) X_{x,y} \\ & + a_{x+1,y \rightarrow x,y} X_{x+1,y} + a_{x,y+1 \rightarrow x,y} X_{x,y+1} = 0, \end{aligned} \quad (\text{A6})$$

with $a = r^4$ and $X = P$ for the hydraulic case, and $a = r^2$ et $X = V$ for the electrical case. For the nodes on the border of the network, eq. (A6) is easily modified to take into account the boundary conditions as described in Fig. 1. A linear system is obtained; the $N_x N_y$ unknowns are the hydraulic pressure or electrical potential at the nodes of the network. Once this system is solved, the modified fluxes can be computed using eqs (A2) and (A4). We used a QR decomposition to invert the matrix, which works even though the

matrix is singular (for instance, when the four tubes connected to a given nodes are equal to zero).

The ‘apparent’ permeability of the network is then computed using Darcy's law:

$$k_{\text{app}} = \frac{\eta Q L}{S |\Delta P|} = \frac{\eta}{l^2} \frac{N_y - 1}{N_x - 1} \frac{\Phi_{\Sigma \text{out/in}}^h}{|\Delta P|}, \quad (\text{A7})$$

where L is the length of the network along the flow direction (i.e. y -direction), S the transversal section, and the total out-flowing and in-flowing modified fluxes are given by

$$\begin{cases} \Phi_{\Sigma \text{out}}^h = \sum_{x=1}^{N_x-1} \Phi_{x,N_y-1 \rightarrow x,N_y}^h \\ \Phi_{\Sigma \text{in}}^h = \sum_{x=1}^{N_x-1} \Phi_{x,1 \rightarrow x,2}^h \end{cases}. \quad (\text{A8})$$

For a fully saturated network ($S_w = 1$), k_{app} is equal to the true permeability of the medium, denoted k . For unsaturated medium, it is convenient to introduce the relative permeability k_r , comprised and 0 and 1. It is defined as

$$k_{\text{app}}(S_w) = k_r(S_w) k \quad (\text{A9})$$

Therefore, introducing eq. (A7) into eq. (A9), the relative permeability is computed by

$$k_r(S_w) = \frac{\Phi_{\Sigma \text{out/in}}^h(S_w)}{\Phi_{\Sigma \text{out/in}}^h(S_w = 1)} \quad (\text{A10})$$

The ‘apparent’ formation factor of the network is computed using

$$\frac{1}{F_{\text{app}}} = \frac{\sigma_r}{\sigma_w} = \frac{1}{\sigma_w} \frac{J L}{S |\Delta V|} = \frac{1}{l^2} \frac{N_y - 1}{N_x - 1} \frac{\Phi_{\Sigma \text{out/in}}^e}{|\Delta V|} \quad (\text{A11})$$

It is here convenient to introduce the resistivity index RI, defined by

$$\text{RI} = \frac{\rho(S_w)}{\rho(S_w = 1)}, \quad (\text{A12})$$

where ρ is the true resistivity of the medium. Replacing the resistivity by the conductivity, introducing the definition of the formation factor and using eq. (A11), RI is computed by

$$\text{RI} = \frac{\Phi_{\Sigma \text{out/in}}^e(S_w = 1)}{\Phi_{\Sigma \text{out/in}}^e(S_w)} \quad (\text{A13})$$

Finally, we computed the two characteristic lengths (the first one, Λ_h , is based on the hydraulic potential, and the second one, Λ_e , on the electrical potential), as defined in Schwartz *et al.* (1989) using the formula given in Bernabé & Revil (1995):

$$\Lambda_h = \frac{\sum_{i=1}^{N_t} r_i^2 |\Delta P_i|^2}{\sum_{i=1}^{N_t} r_i |\Delta P_i|^2} \quad (\text{A14})$$

and

$$\Lambda_e = \frac{\sum_{i=1}^{N_t} r_i^2 |\Delta V_i|^2}{\sum_{i=1}^{N_t} r_i |\Delta V_i|^2}, \quad (\text{A15})$$

where ΔP_i (resp. ΔV_i) is the hydraulic pressure (resp. electrical potential) difference between the two end nodes of the i th tube.